IEEE Access
Multidisciplinary ⋮ Rapid Review ⋮ Open Access Journal

Received August 23, 2019, accepted September 12, 2019, date of publication September 16, 2019,
date of current version September 27, 2019.

Digital Object Identifier 10.1109/ACCESS.2019.2941775

Autocorrelation Function of Full-Response CPM Signals and Its Application to Synchronization

ZHENGGUANG XU[1] AND QIFENG WANG[2]
[1]School of Electronic Information and Communication, Huazhong University of Science and Technology, Wuhan 430074, China
[2]School of Electronic and Information Engineering, Wuhan Donghu University, Wuhan 430212, China

Corresponding author: Qifeng Wang (q.f.wang1978@qq.com)

This work was supported by the Hubei Provincial Natural Science Foundation of China under Grant 2017CFB803.

ABSTRACT Two types of the autocorrelation functions of the full-response continuous phase modulation (CPM) signal are investigated in the paper, the autocorrelation functions are proven to be periodic functions when the modulation index of the CPM signal is $h = 1$. Then the autocorrelation functions are expanded in the form of Fourier series, and two synchronization schemes are proposed to estimate the synchronization parameters from the coefficients of the Fourier series, including the carrier frequency offset, the carrier phase and the timing offset. The performances of the synchronization algorithms are shown by simulations and compared with the modified Cramer-Rao bounds (MCRB) and other synchronization schemes. The simulation results show that the first type of the proposed scheme has better synchronization performances than the available schemes.

INDEX TERMS Synchronization, frequency estimation, phase estimation, timing recovery, continuous phase modulation.

I. INTRODUCTION

Continuous phase modulation (CPM) is a bandwidth efficient digital modulation scheme used for data transmission over band-limited channels [1]. Since the statistical parameters of the CPM signals do not contain the transmitted symbol information, the statistical characteristics of the CPM signals could be used to estimate the modulation parameters and synchronization parameters. In [2], the first-order statistics of the CPM signals are investigated to estimate the modulation parameters of the CPM signal, including modulation index, the symbol period and the frequency offset. In [3], the second-order statistics of the CPM signals are investigated to describe the power spectral density function. In [4], the first-order and second-order statistics are both used to solve the synchronization problem of the CPM signal. The synchronization procedure includes carrier frequency and phase estimation, timing recovery, which are necessary in the CPM receiver and there are many research works on the issues [5].

The synchronization schemes can be divided into data-aided and non-data-aided schemes. In [6] and [7], the data-aided schemes are investigated and the recovery performance is close to the modified Cramer-Rao bound (MCRB) [8], but the training sequence must be inserted into the transmitted sequence so that the spectral efficiency decreases. Therefore, more research works focus on the non-data-aided schemes where the schemes could be divided into decision-feedback and feedforward structures. The decision-feedback scheme utilizes the symbol decision results to help the synchronization procedure [9]. The feedforward scheme is the open loop and the synchronization procedure is implemented independently with demodulation process [10]. Therefore, the feedforward scheme is simpler than that of the feedback scheme, and easy to implement.

Among the feedforward schemes in the available literatures, the common viewpoint that all the algorithms use the characteristics of the CPM signals with $h = 1$. In [11], the algorithm is designed for the CPM signal with $h = 1$. In [12] and [13], the square operation is used to convert $h = 1/2$ into $h = 1$. However, the statistical characteristics of the CPM signal with $h = 1$ are not investigated in those literatures. In [4], some statistics are discussed and used to design the synchronization algorithm, but the autocorrelation functions of the CPM signal are not considered.

In the paper, we investigate the characteristics of the autocorrelation function of the CPM signal with $h = 1$. For simplicity, we restrict ourselves to full-response CPM [14], i.e., those with pulse length equal to the symbol period.

The associate editor coordinating the review of this manuscript and approving it for publication was Wu-Shiung Feng.

Extensions to other pulse length are possible but, for space limitations, are not pursued here.

The paper is organized as follows. In Section II, we describe the autocorrelation functions of CPM with $h = 1$ and provide the brief proofs. In Section III, we derive the joint estimators from the characteristics respectively. The numerical results are provided in Section IV and conclusions are summarized in Section V.

II. AUTOCORRELATION FUNCTIONS OF THE CPM

The complex envelope of the CPM is

$$s(t) = e^{j\phi(t)} \tag{1}$$

where the modulated phase is [1]

$$\phi(t) = 2\pi h \sum_{k=0}^{n} \alpha_k q(t - kT). \tag{2}$$

In the phase definition, h is the modulation index, T is the symbol period, and α_k are independent binary data symbols, each taking one of the values

$$\alpha_k = \pm 1 \tag{3}$$

with equal probability $1/2$. Therefore, we have

$$E\{\alpha_k\} = 0. \tag{4}$$

Here $E\{\cdot\}$ denotes expectation operation to α_k. The function $q(t)$ is the phase pulse of the modulator, which is related to the frequency pulse $g(t)$ by the relationship

$$q(t) = \int_{-\infty}^{t} g(\tau)\, d\tau. \tag{5}$$

For full-response CPM signals, $g(t)$ is time-limited to the interval $(0, T)$ and satisfies $g(t) = g(T - t)$. Therefore,

$$q(t) = \begin{cases} 0, & t \le 0; \\ 1/2 - q(T - t), & 0 < t < T; \\ 1/2, & t \ge T. \end{cases} \tag{6}$$

Usually we consider two frequency pulses: rectangular pulse (REC) and raised-cosine (RC) pulse as follows.

$$g(t) = \frac{1}{2T}, \quad \text{with REC}, \tag{7}$$

$$g(t) = \frac{1}{2T}\left(1 - \cos\frac{2\pi t}{T}\right), \quad \text{with RC}. \tag{8}$$

which are both time-limited to the interval $(0, T)$. In the two cases, $q(t)$ are shown in Fig. 1.

In the paper, we define two types of the correlation functions of the CPM signals as follows

$$F^{+}(t, \Delta t) = E[s(t)\, s(t - \Delta t)] \tag{9}$$

and

$$F^{-}(t, \Delta t) = E\left[s(t)\, s^{*}(t - \Delta t)\right] \tag{10}$$

where "*" denotes conjugation operation.

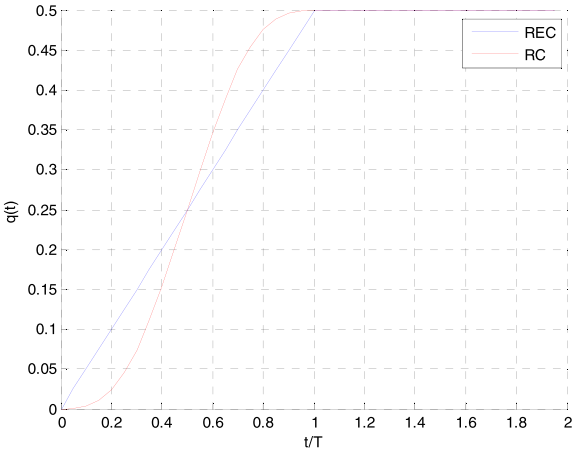

FIGURE 1. The curves of $q(t)$.

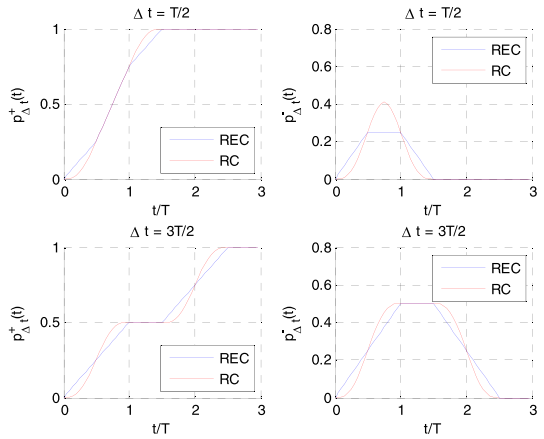

FIGURE 2. The curves of $p_{\Delta t}^{\pm}(t)$ with REC and RC pulses.

Letting

$$p_{\Delta t}^{\pm}(t) = q(t) \pm q(t - \Delta t) \tag{11}$$

for $h = 1$ we obtain

$$\begin{aligned} F^{\pm}(t, \Delta t) &= \prod_{n=0}^{\infty} E\left[e^{j2\pi\alpha_n p_{\Delta t}^{\pm}(t - nT)}\right] = \prod_{n=0}^{\infty} \cos 2\pi p_{\Delta t}^{\pm}(t - nT) \\ &= \cos 2\pi p_{\Delta t}^{\pm}(t) \prod_{n=0}^{\infty} \cos 2\pi p_{\Delta t}^{\pm}(t - (n+1)T) \\ &= \cos 2\pi p_{\Delta t}^{\pm}(t)\, F^{\pm}(t - T, \Delta t) \end{aligned} \tag{12}$$

Considering $p_{\Delta t}^{+}(t) = 1$ and $p_{\Delta t}^{-}(t) = 0$ for $t > T + \Delta t$, so

$$\cos 2\pi p_{\Delta t}^{\pm}(t) = 1. \tag{13}$$

Therefore,

$$F^{\pm}(t, \Delta t) = F^{\pm}(t - T, \Delta t) \tag{14}$$

which means $F^{\pm}(t, \Delta t)$ are the real periodic functions with period T. The curves of $p_{\Delta t}^{\pm}(t)$ are shown in Fig. 2. The curves of $F^{\pm}(t, \Delta t)$ with different Δt are shown in Fig. 3.

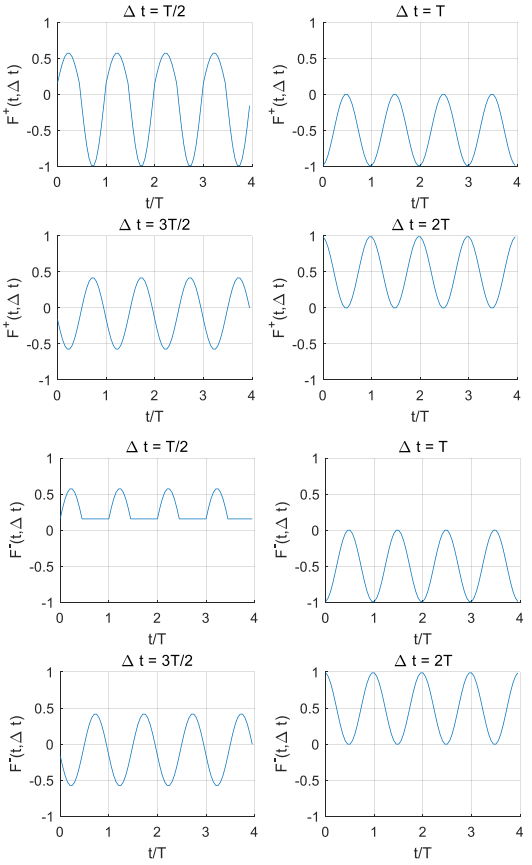

FIGURE 3. The curves of $F^{\pm}(t, \Delta t)$ with REC pulse.

Expand $F^{\pm}(t, \Delta t)$ in the Fourier series as follows

$$F^{\pm}(t, \Delta t) = \sum_{m=-\infty}^{\infty} c_m^{\pm}(\Delta t)\, e^{j2m\pi t/T} \tag{15}$$

where

$$c_m^{\pm}(\Delta t) = \frac{1}{T}\int_0^T F^{\pm}(t, \Delta t)\, e^{-j2m\pi t/T} dt \tag{16}$$

are the Fourier coefficients controlled by Δt. For REC pulse, the curves of $\left|c_m^{\pm}(\Delta t)\right|$ are shown in Fig.4. When $\left|c_m^{\pm}(\Delta t)\right|$ is larger, the energy of the corresponding frequency component is larger and the anti-noise ability is better. Therefore, we usually choose larger $\left|c_m^{\pm}(\Delta t)\right|$ in the following synchronization algorithm.

III. SYNCHRONIZATION SCHEMES

The complex envelope of the CPM signal with the frequency offset and timing offset is

$$x(t) = e^{j(2\pi vt+\theta)} s(t-\tau) \tag{17}$$

where v is the frequency offset, θ is the carrier phase and τ is the timing offset. The three parameters are unknown, so the synchronization algorithms are designed to estimate the parameters. Now we provide two schemes from the two autocorrelation functions described in the last section.

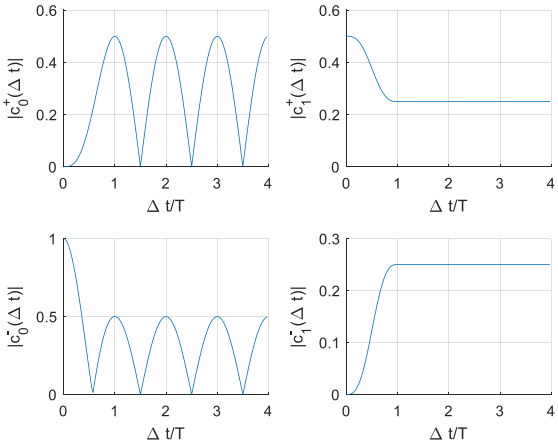

FIGURE 4. The curves of $\left|c_m^{\pm}(\Delta t)\right|$.

Considering

$$\begin{aligned} &E[x(t)\, x(t-\Delta t)] \\ &\quad = e^{j(4\pi vt-2\pi v\Delta t+2\theta)} E[s(t-\tau)\, s(t-\tau-\Delta t)] \\ &\quad = e^{j(4\pi vt-2\pi v\Delta t+2\theta)} F^{+}(t-\tau, \Delta t) \end{aligned} \tag{18}$$

we substitute (15) into (18) and obtain

$$\begin{aligned} &E[x(t)\, x(t-\Delta t)] \\ &= e^{j(4\pi vt-2\pi v\Delta t+2\theta)} \sum_{m=-\infty}^{\infty} c_m^{+}(\Delta t)\, e^{j2m\pi(t-\tau)/T}. \end{aligned} \tag{19}$$

Considering the Fourier transform of $E[x(t)\, x(t-\Delta t)]$

$$\begin{aligned} S^{+}(f, \Delta t) &= \int_0^T E[x(t)\, x(t-\Delta t)]\, e^{-j2\pi ft} dt \\ &= e^{j(-2\pi v\Delta t-2m\pi\tau/T+2\theta)} \sum_{m=-\infty}^{\infty} c_m^{+}(\Delta t) \\ &\quad \times \int_0^T e^{j2\pi(2v+m/T-f)t} dt \end{aligned} \tag{20}$$

For $f = 2v + k/T$, we obtain

$$S^{+}(2v + k/T, \Delta t) = c_k^{+}(\Delta t)\, Te^{j(2\theta-2\pi v\Delta t-2k\pi\tau/T)}. \tag{21}$$

The formula (21) shows the relationship between the synchronization parameters and the discrete spectral lines $S^{+}(2v + k/T, \Delta t)$. Obviously, the distribution of the spectral lines is centered on $2v$ with the interval $1/T$ and the amplitudes of the spectral lines depend on $\left|c_k^{+}(\Delta t)\right|$. When we locate the spectral lines in the frequency domain, the frequency offset v is obtained. Then the timing offset τ and the carrier phase θ could be estimated from the argument of the spectral lines. Therefore, the synchronization parameters could be obtained as follows

$$v = \frac{1}{2}\arg\max\left(\left|S^{+}(f, \Delta t)\right|\right), \tag{22}$$

$$\tau = -\frac{T}{4k\pi}\arg\frac{S^{+}(2v+k/T, \Delta t)}{c_k^{+}(\Delta t)}\left(\frac{S^{+}(2v-k/T, \Delta t)}{c_{-k}^{+}(\Delta t)}\right)^{*}, \tag{23}$$

$$\theta = \frac{1}{4}\arg\frac{S^+(2v+k/T,\Delta t)\,S^+(2v-k/T,\Delta t)\,e^{j4\pi v\Delta t}}{c_k^+(\Delta t)\,c_{-k}^+(\Delta t)}. \tag{24}$$

Here $c_k^+(\Delta t)$ could be calculated by (16), and $S^+(f,\Delta t)$ could be calculated by (20). However, $E[x(t)\,x(t-\Delta t)]$ in (20) is difficult to obtain in the practical application, so we calculate

$$S^+(f,\Delta t) = \int_0^{NT} x(t)\,x(t-\Delta t)\,e^{-j2\pi ft}dt \tag{25}$$

where N is the number of the observed symbol. When N is large enough, the time averages could be used instead of statistical averages.

Considering

$$\begin{aligned} E\left[x(t)\,x^*(t-\Delta t)\right] &= e^{j2\pi v\Delta t}E\left[s(t-\tau)\,s^*(t-\tau-\Delta t)\right] \\ &= e^{j2\pi v\Delta t}F^-(t-\tau,\Delta t) \end{aligned} \tag{26}$$

we substitute (15) into (26) and obtain

$$E\left[x(t)\,x^*(t-\Delta t)\right] = e^{j2\pi v\Delta t}\sum_{m=-\infty}^{\infty} c_m^-(\Delta t)\,e^{j2m\pi(t-\tau)/T}. \tag{27}$$

The Fourier transform of $E\left[x(t)\,x^*(t-\Delta t)\right]$ is

$$\begin{aligned} S^-(f,\Delta t) &= \int_0^T E\left[x(t)\,x^*(t-\Delta t)\right]e^{-j2\pi ft}dt \\ &= e^{j(2\pi v\Delta t-2m\pi\tau/T)}\sum_{m=-\infty}^{\infty} c_m^-(\Delta t) \\ &\quad\times\int_0^T e^{j2\pi(m/T-f)t}dt \end{aligned} \tag{28}$$

For $f = k/T$, we obtain

$$S^-(k/T,\Delta t) = c_k^-(\Delta t)\,Te^{j(2\pi v\Delta t-2k\pi\tau/T)} \tag{29}$$

The formula (29) shows the relationship between the synchronization parameters and the discrete spectral lines $S^-(k/T,\Delta t)$. Different from (21), the spectral lines are distributed around the zero frequency with the interval $1/T$, so we cannot find the frequency offset v by searching the peak. The carrier phase is not included in (29), so we cannot estimate the carrier phase. However, we could estimate the frequency offset and the timing offset from the argument of $S^-(k/T,\Delta t)$ as follows

$$v = \frac{1}{2\pi\Delta t}\arg\frac{S^-(0,\Delta t)}{c_0^-(\Delta t)} \tag{30}$$

$$\tau = -\frac{T}{4k\pi}\arg\frac{S^-(k/T,\Delta t)}{c_k^-(\Delta t)}\left(\frac{S^-(-k/T,\Delta t)}{c_{-k}^-(\Delta t)}\right)^* \tag{31}$$

Similar, $S^-(k/T,\Delta t)$ is calculated by

$$S^-(f,\Delta t) = \int_0^{NT} x(t)\,x^*(t-\Delta t)\,e^{-j2\pi ft}dt \tag{32}$$

Now we have presented two types of synchronization schemes from the two definitions of autocorrelation. However, the parameters Δt and k are not provided in (22)-(24) and (30)-(31). In the noise-free environment, any Δt and k that ensure $c_k^{\pm}(\Delta t) \neq 0$ could be used to estimate the synchronization parameters. However, in the practical environment with additive white Gaussian noise (AWGN), we should choose larger $\left|c_k^{\pm}(\Delta t)\right|$ to ensure larger signal-to-noise ratio (SNR).

For the first autocorrelation (AC1) scheme in (22)-(24), the frequency offset is estimated at $k = 0$. As shown in Fig. 4, the curve of $\left|c_0^+(\Delta t)\right|$ achieves the maximum at $\Delta t = mT$ $(m \neq 0)$, so we could rewrite the formula (22) as follows

$$v = \frac{1}{2M}\sum_{m=1}^{M}\arg\max\left(\left|S^+(f,mT)\right|\right) \tag{33}$$

where the average frequency offset is calculated by M different Δt to improve the accuracy of the estimator. Then we estimate the other two parameters by (23) and (24) at $k = 1$ and $\Delta t = T$.

For the second autocorrelation (AC2) scheme in (30)-(31), the frequency offset is also estimated at $k = 0$. As shown in Fig. 4, the curve of $\left|c_0^-(\Delta t)\right|$ achieves the maximum at $\Delta t = mT$, so we could rewrite the formula (30) as follows

$$v = \frac{1}{M}\sum_{m=1}^{M}\frac{1}{2m\pi\,\Delta t}\arg\frac{S^-(0,m\Delta t)}{c_0^-(m\Delta t)} \tag{34}$$

Similar, we could rewrite the formula (31) as follows

$$\tau = -\frac{1}{M}\sum_{m=1}^{M}\frac{T}{4\pi}\arg\frac{S^-(1/T,m\Delta t)}{c_1^-(m\Delta t)}\left(\frac{S^-(-1/T,m\Delta t)}{c_{-1}^-(m\Delta t)}\right)^* \tag{35}$$

The two schemes above are designed for the CPM signals with $h = 1$. For the CPM signal with arbitrary modulation index, the phase unwrapping technique could be used to convert the modulation index into 1, which is described in [4], so we just consider the case of $h = 1$ in the paper. In the first autocorrelation (AC1) scheme, we search the frequency domain to find the frequency offset, and then calculate the timing offset and carrier phase. In the second autocorrelation (AC2) scheme, we calculate the frequency offset and the timing offset independently. In the next section, we will compare the estimation performances of the two schemes by numerical simulations.

IV. NUMERICAL SIMULATIONS

In this section, we show the simulation results for CPM signals with rectangular (REC) and raised-cosine (RC) frequency pulses.

For the discrete-time implementation, the sampling rate $f_s = 4/T$ is used. The incoming waveform is first fed to a lowpass filter to eliminate out-of-band noise, which is

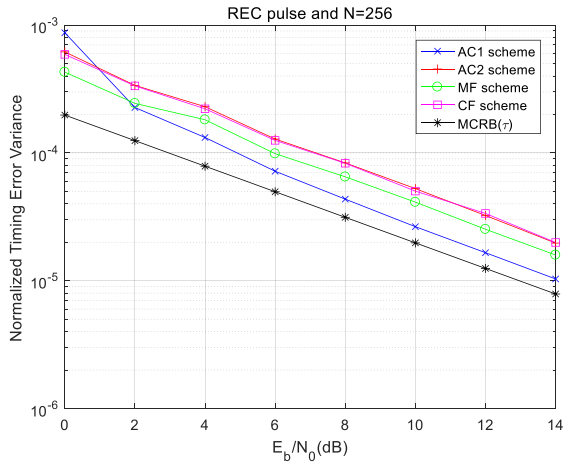

(a) Timing MSE

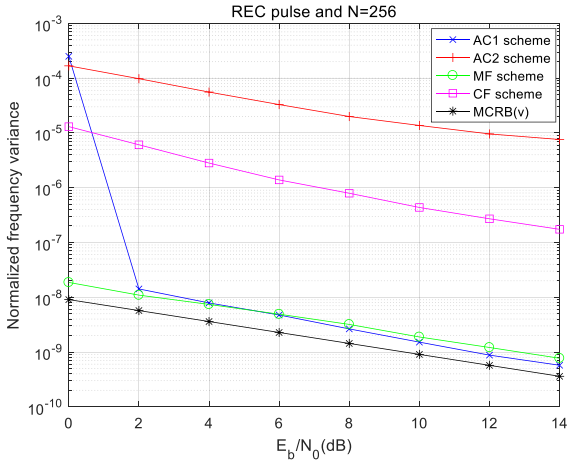

(b) Frequency MSE

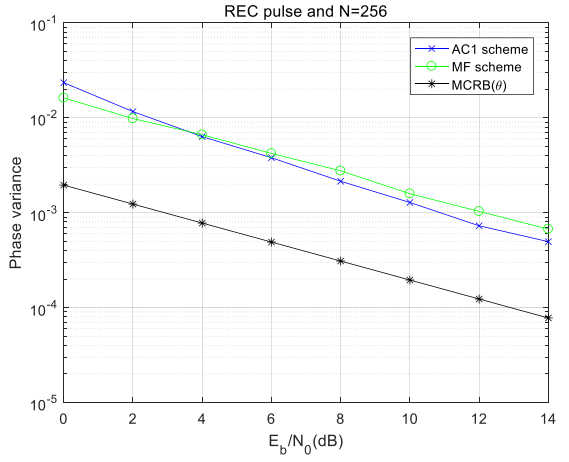

(c) Phase MSE

FIGURE 5. Performance comparison for REC pulse and N = 256.

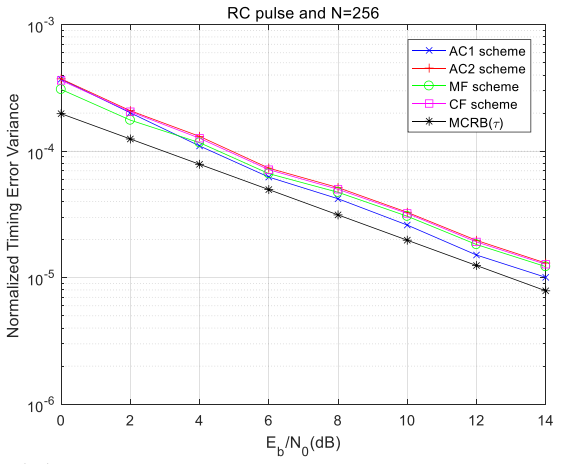

(a) Timing MSE

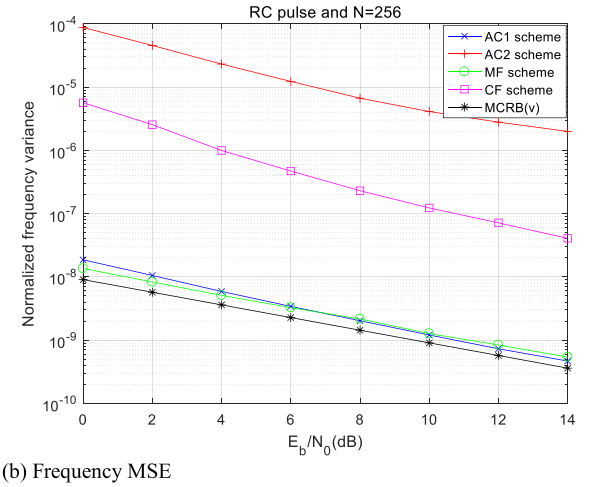

(b) Frequency MSE

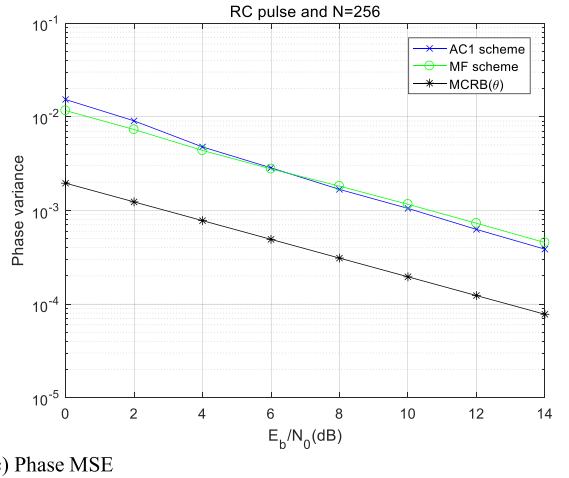

(c) Phase MSE

FIGURE 6. Performance comparison for RC pulse and $N = 256$.

produced by the Matlab filter design function 'fir1'. The order of the filter is 20 and its bandwidth is $1/T$. There are 2000 Monte-carlo simulations in each figure. In all the simulations, the average parameter in (33), (34) and (35) are $M = 4$. The number of the observed symbol is $N = 256$.

The normalized timing, frequency and phase mean square errors (MSEs) as a function of E_s/N_0 are shown in the simulations. The tight bounds of the two schemes are difficult to obtain, so we just compare the performances with the modified Cramer–Rao bounds (MCRBs), which are usually used as benchmark in all the available literatures. They are

expressed by [5]

$$MCRB(\tau) = \begin{cases} \dfrac{T}{2\pi^2 N (E_s/N_0)}, & \text{with REC;} \\ \dfrac{T}{3\pi^2 N (E_s/N_0)}, & \text{with RC;} \end{cases} \quad (36)$$

$$MCRB(v) = \frac{3}{2\pi^2 T^2 N^3 (E_s/N_0)} \quad (37)$$

$$MCRB(\theta) = \frac{1}{2N (E_s/N_0)} \quad (38)$$

The estimation performances for CPM signals with REC frequency pulse are shown in Fig. 5. In order to evaluate the performance of the proposed schemes, we compare the proposed scheme with two schemes in [4], the MF scheme is based on the mean-function of the CPM signal, and the CF scheme is based on the correlation function of the CPM signal, which is a little similar with the AC2 schemes but the estimation formulas are different. The three subfigures show the timing, frequency and phase estimation performances respectively.

In Fig. 5a, the AC1 scheme has the best performance and its timing MSE is far from the MCRB about 1dB. The AC2 scheme and the CF scheme have the similar performance since they are both based on the traditional correlation function at $\Delta t = mT$. In Fig. 5b, the performances of the AC1 scheme and the MF scheme are close to the MCRB in high SNR, but the performances of the AC2 scheme and the CF scheme are far from the MCRB since the two schemes calculate the frequency offset from the argument, which is more susceptible to noise than the amplitude in the frequency domain. Fig. 5c shows the phase MSE of the AC1 and MF schemes, and the AC2 and CF schemes cannot estimate the carrier phase, since the traditional correlation function does not include the carrier phase information. The performance of the AC1 scheme is better than that of the MF scheme in high SNR.

The estimation performances for CPM signals with RC frequency pulse and $h = 1$ are shown in Fig. 6. The conclusions are similar to the case with REC pulse, and the AC1 scheme has the best performance. It is because the algorithms are designed for all the full-response CPM signals with $h = 1$ regardless of the pulse type. Therefore, the proposed schemes could be generalized to any pulse type.

In Figs. 5-6, the simulation results indicate that both the schemes can provide the synchronization parameters for full-response CPM signal. However, the AC1 scheme has the best performance among the schemes and its MSEs are close to the MCRB in high SNR.

V. CONCLUSION

In the paper, we investigate the property of the two types of the autocorrelation functions for full-response CPM signals with $h = 1$. Based on the property, the joint frequency and timing recovery schemes are discussed for binary full-response CPM signals with $h = 1$. The performances of the schemes are compared in the numerical simulations and the first type of the scheme shows the best performances.

REFERENCES

[1] A. Barbieri, D. Fertonani, and G. Colavolpe, "Spectrally-efficient continuous phase modulations," *IEEE Trans. Wireless Commun.*, vol. 8, no. 3, pp. 1564–1572, Mar. 2009.
[2] P. Bianchi, P. Loubaton, and F. Sirven, "On the blind estimation of the parameters of continuous phase modulated signals," *IEEE J. Sel. Areas Commun.*, vol. 23, no. 5, pp. 944–962, May 2005.
[3] A. Napolitano and C. M. Spooner, "Cyclic spectral analysis of continuous-phase modulated signals," *IEEE Trans. Signal Process.*, vol. 49, no. 1, pp. 30–44, Jan. 2001.
[4] X. Xie and Z. Xu, "Comparison of feedforward synchronization schemes for full-response CPM signals," *IEEE Access*, vol. 5, pp. 27376–27383, 2017.
[5] U. Mengali and A. N. D'Andrea, *Synchronization Techniques for Digital Receivers*. New York, NY, USA: Plenum Press, 1997.
[6] J. Huber and W. Liu, "Data-aided synchronization of coherent CPM-receivers," *IEEE Trans. Commun.*, vol. 40, no. 1, pp. 178–189, Jan. 1992.
[7] E. Hosseini and E. Perrins, "Timing, carrier, and frame synchronization of burst-mode CPM," *IEEE Trans. Commun.*, vol. 61, no. 12, pp. 5125–5138, Dec. 2013.
[8] A. N. D'Andrea, U. Mengali, and R. Reggiannini, "The modified Cramer–Rao bound and its application to synchronization problems," *IEEE Trans. Commun.*, vol. 42, nos. 2–4, pp. 1391–1399, Feb./Apr. 1994.
[9] L. Wang, J. Qi, and P. Song, "A simplified direct-decision synchronization algorithm for coherent CPM receiver using linear phase approximation," *IEEE Commun. Lett.*, vol. 23, no. 1, pp. 100–103, Jan. 2019.
[10] X. Xie and Z. Xu, "Feedforward joint frequency and timing estimation scheme for M-CPFSK signals," *Electron. Lett.*, vol. 52, no. 10, pp. 876–877, May 2016.
[11] G. Caire and C. Elia, "A new symbol timing and carrier frequency offset estimation algorithm for noncoherent orthogonal M-CPFSK," *IEEE Trans. Commun.*, vol. 45, no. 10, pp. 1314–1326, Oct. 1997.
[12] R. Mehlan, Y.-E. Chen, and H. Meyr, "A fully digital feedforward MSK demodulator with joint frequency offset and symbol timing estimation for burst mode mobile radio," *IEEE Trans. Veh. Technol.*, vol. 42, no. 4, pp. 434–443, Nov. 1993.
[13] M. Morelli and U. Mengali, "Joint frequency and timing recovery for MSK-type modulation," *IEEE Trans. Commun.*, vol. 47, no. 6, pp. 938–946, Jun. 1999.
[14] T. Aulin and C. E. Sundberg, "Continuous phase modulation—Part I: Full response signaling," *IEEE Trans. Commun.*, vol. COMM-29, no. 3, pp. 196–209, Mar. 1981.

ZHENGGUANG XU received the bachelor's degree in communication engineering, the master's degree in communication and information system, and the Ph.D. degree in information and communication engineering from the Huazhong University of Science and Technology, China, in 2004, 2006, and 2009, respectively, where he is currently an Associate Professor with the School of Electronic Information and Communications. His research interests include signal processing, wireless communication, and data analysis.

QIFENG WANG received the Ph.D. degree in information and communication engineering from the Huazhong University of Science and Technology, China, in 2016. He is currently with the School of Electronic and Information Engineering, Wuhan Donghu University, China. His current research interests include signal processing, parameter estimation, communication system simulation, and cognitive radio.